Diao, F., Xiong, X., Wang, R., Walter, T. R., Wang, Y., Wang, K. (2019): Slip Rate Variation Along the Kunlun Fault (Tibet): Results From New GPS Observations and a Viscoelastic Earthquake-Cycle Deformation Model. - *Geophysical Research Letters*, *46*, 5, pp. 2524—2533.

DOI: http://doi.org/10.1029/2019GL081940

Geophysical Research Letters

RESEARCH LETTER
10.1029/2019GL081940

Key Points:
- The slip rate of the Tuosuo Lake segment (Kunlun fault) is estimated to be 5.5 ± 0.7 mm/a using new data from a dense GPS profile
- The slip rate of the Kunlun fault likely decreases from the Tuosuo Lake segment toward its eastern tip
- Viscoelastic relaxation during the earthquake cycle has a significant effect on the geodetic estimation of fault slip rate

Supporting Information:
- Supporting Information S1

Correspondence to:
F. Diao,
fqdiao@cug.edu.cn

Citation:
Diao, F., Xiong, X., Wang, R., Walter, T. R., Wang, Y., & Wang, K. (2019). Slip Rate Variation Along the Kunlun Fault (Tibet): Results From New GPS Observations and a Viscoelastic Earthquake-Cycle Deformation Model. *Geophysical Research Letters*, *46*, 2524–2533. https://doi.org/10.1029/2019GL081940

Received 7 JAN 2019
Accepted 26 FEB 2019
Accepted article online 1 MAR 2019
Published online 13 MAR 2019

Slip Rate Variation Along the Kunlun Fault (Tibet): Results From New GPS Observations and a Viscoelastic Earthquake-Cycle Deformation Model

Faqi Diao[1], Xiong Xiong[1], Rongjiang Wang[2], Thomas R. Walter[2], Yuebing Wang[3], and Kai Wang[4]

[1]Hubei Subsurface Multi-Scale Imaging Key Laboratory, Institute of Geophysics and Geomatics, China University of Geosciences, Wuhan, China, [2]GFZ German Research Centre for Geosciences, Potsdam, Germany, [3]China Earthquake Networks Center, Beijing, China, [4]State Key Laboratory of Geodesy and Earth's Dynamics, Institute of Geodesy and Geophysics, Chinese Academy of Sciences, Wuhan, China

Abstract The slip rate and its spatial variations of the Kunlun fault (KLF) play important roles in the tectonic evolution of the northeastern Tibetan Plateau. Here the slip rate of the Tuosuo Lake (TL) segment of the KLF, which remains controversial from various geological observations, is investigated with a dense Global Positioning System observation profile. With a viscoelastic earthquake-cycle deformation model, the slip rate of the TL segment is estimated to be 5.5 ± 0.7 mm/a, in comparison with an overestimated value of 9.2 ± 1.1 mm/a from an elastic model. Combined with previous results, we infer that the slip rate of the KLF likely decreases gradually from the TL segment toward the eastern tip, rather than remaining uniform along the fault or decreasing rapidly within the easternmost 150 km. The estimated lower crust viscosity (~10^{18} Pa · s) agrees with values inferred from postseismic studies, which suggests a weak ductile lower crust in this region.

Plain Language Summary The Kunlun fault (KLF) is one of the major left-lateral strike-slip faults on the Tibetan Plateau and accommodates a significant portion of the plateau's eastward motion. The slip rate and its spatial variations along the KLF play important roles in understanding the associated tectonic evolution, crustal deformation, and seismic activity. However, how the slip rate varies along the fault remains controversial. Here a dense Global Positioning System velocity profile across the Tuosuo Lake segment is used to probe the slip rate of the eastern KLF. The results inferred from a viscoelastic earthquake-cycle deformation model suggest that the slip rate of the KLF decreases gradually from the Tuosuo Lake segment toward its eastern tip, rather than remaining uniform along the fault or decreasing rapidly within the easternmost 150 km of the fault as inferred previously from different observations. Our results also highlight the viscoelastic relaxation effect during the earthquake cycle.

1. Introduction

The slip rates and their spatial variations along continental faults are important for understanding regional tectonic evolution, crustal deformation, and seismic activity (Duvall & Clark, 2010; Segall & Pollard, 1980; Xiong et al., 2010; Zheng et al., 2013). Spatial variations of fault slip rate have been observed on many major continental faults, which highlight the complexity of fault frictional behavior, geometric configuration, and segmentation (Cowie & Scholz, 1992; Diao et al., 2016; Hubbard et al., 2016; Manighetti et al., 2007). Here we investigate the eastern Kunlun fault (KLF) in northeastern region of the Tibetan Plateau, which is well suited for investigations of fault behavior in terms of slip rate variation and interaction with other large faults. Along its entire ~1,600-km length, the KLF separates the Qidam block and the Bayan Hor block and accommodates a significant portion of the Tibetan Plateau's eastward motion by fault slip along the strike (Figure 1).

The slip rate along the KLF estimated from geological investigations in recent decades remains controversial, especially for the eastern segments. Van der Woerd et al. (2000, 2002) indicate a uniform slip rate of 11.5 ± 2.0 mm/a along the fault. Kirby et al. (2007) and Lin and Guo (2008) suggest that the slip rate decreases rapidly from >10 to <2 mm/a along ~150 km toward its eastern tip, but recent large-scale

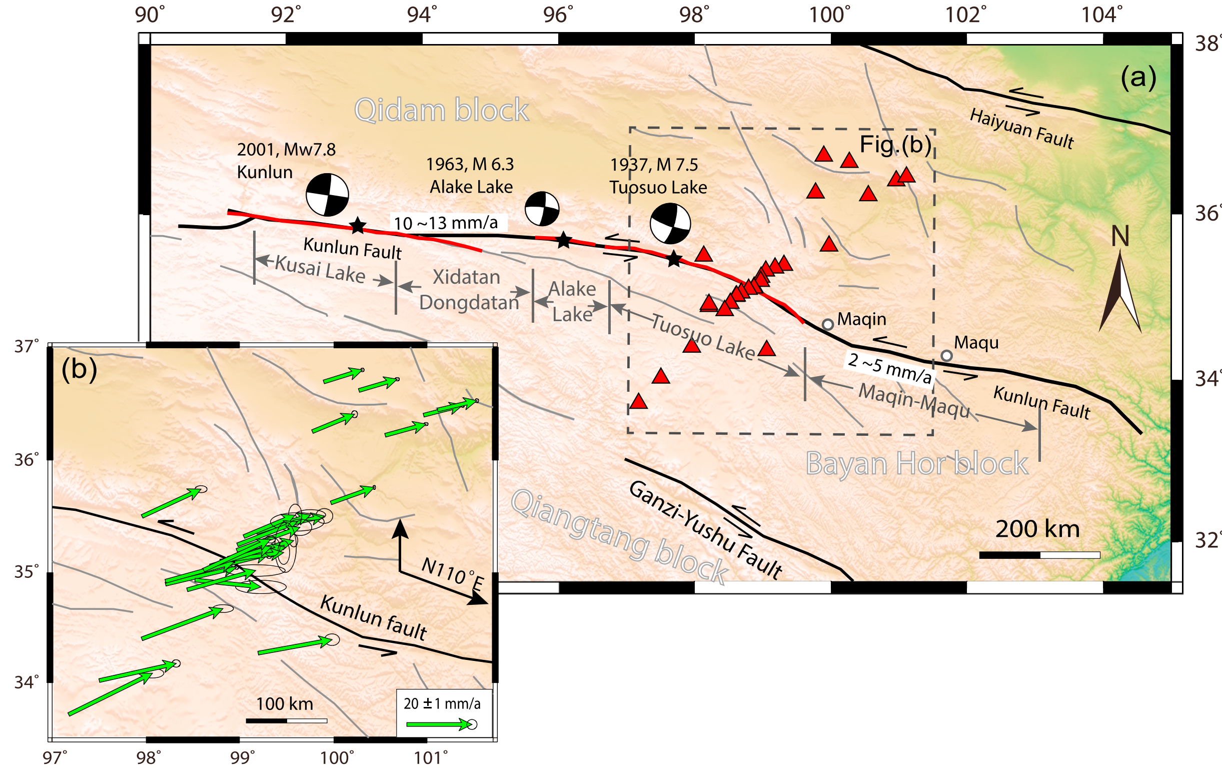

Figure 1. (a) Tectonic setting of the Kunlun fault. The thick red lines and beach balls indicate the surface rupture traces and focal mechanisms of historic earthquakes (Guo et al., 2007). The red triangles within the dashed rectangle show the Global Positioning System stations used in this study. (b) Velocity profile perpendicular to the fault. The green vectors represent horizontal Global Positioning System velocities with 95% confidence interval relative to the stable Eurasian Plate.

geodetic observation reveals gradually decreasing slip rates from the middle to the eastern segments (Duvall & Clark, 2010). The Tuosuo Lake (TL) segment that connects the western fast-slipping segment and the eastern slow-slipping segment (Figures 1 and 2) governs how the slip rate varies along the KLF. Considering the large discrepancy in the published geological slip rates of this segment, for example, 11.5 ± 2.0 mm/a from Van der Woerd et al. (2002) and 6.5 ± 1.1 mm/a from Guo et al. (2007), geodetic constraints are necessary for nailing down the slip rate of the TL segment. However, due to the absence of dense near-field observations, the geodetic slip rate on this fault segment has been only approximately estimated (Duvall & Clark, 2010; Zhang et al., 2004).

Geodetically observed fault deformation reveals not only steady fault slip but also transient effects during an earthquake cycle including coseismic rupture, postseismic deformation, and interseismic strain accumulation. Two physical models that relate fault deformation to the slip rate have been proposed in past decades. One is the elastic *back-slip* model that assumes buried dislocations beneath a locked portion of a fault (Savage & Burford, 1973). The other model is the viscoelastic earthquake-cycle deformation (VECD) model (Savage & Prescott, 1978), which consists of a fault with periodic slip events in an elastic crust overlying a viscoelastic lower crust and upper mantle. By incorporating the viscoelastic effects of the ductile layers, the VECD model can produce time-dependent cross-fault deformation during an earthquake cycle (Dixon et al., 2003; Hilley et al., 2009; Johnson et al., 2007; Meade & Hager, 2004; Pollitz, 2001; Savage, 2000; Savage & Prescott, 1978; Wang et al., 2012).

Here a new Global Positioning System (GPS) observation profile with dense near-field sampling is used to probe the fault slip rate on the TL segment of the KLF. We first use a simple elastic model to investigate whether such a model can explain the data with reasonable parameters. Then, a more realistic VECD model that incorporates the postseismic and interseismic viscoelastic effects is built, and the fault slip rate and the lower crust viscosity are estimated. Finally, we discuss the tectonic implications of the inferred slip rate along the eastern segment of the KLF.

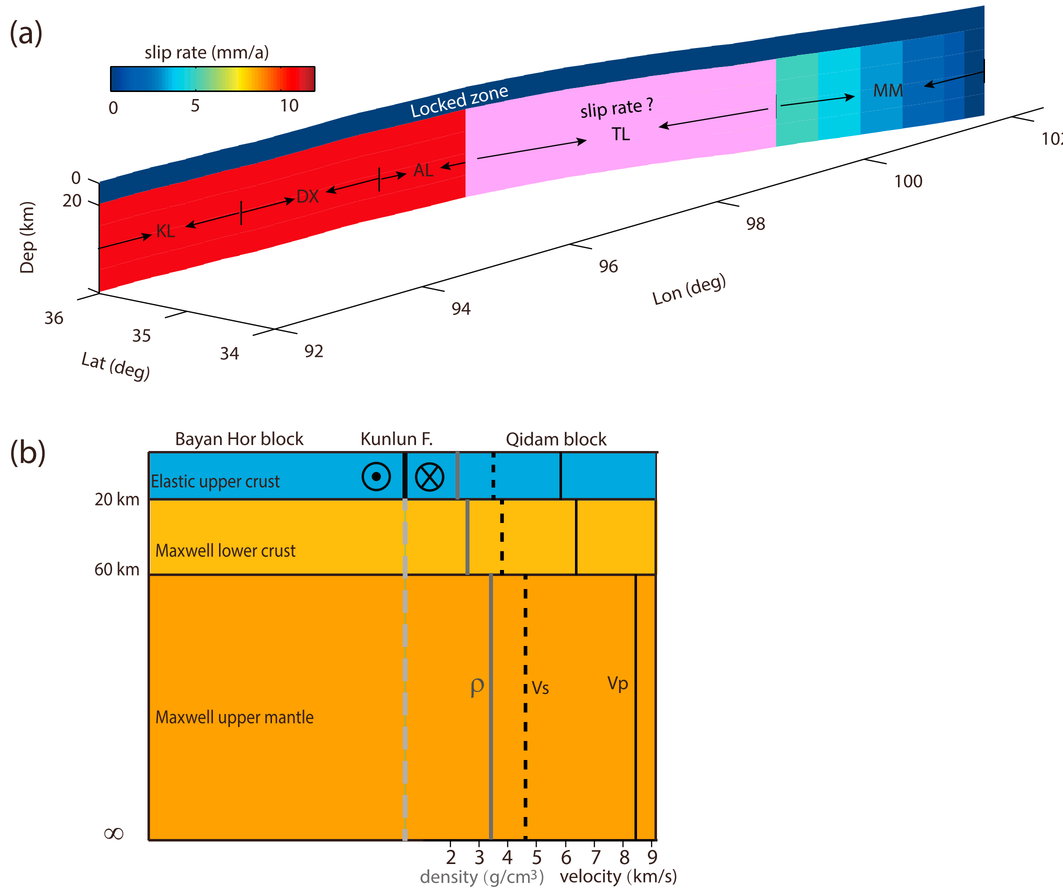

Figure 2. (a) The 3-D fault geometry and segmentation used in the viscoelastic earthquake-cycle deformation model. Abbreviations: KL, Kusai Lake segment; DX, Dongdatan-Xidantan segment; AL, Alake Lake segment; TL, Tuosuo Lake segment; MM, Maqin-Maqu segment. (b) Sketch map and parameter setting of the layered Earth.

2. GPS Data Processing

We use campaign GPS data that were collected between 1999 and 2015 to acquire the interseismic crustal movement in the study area. Only the GPS stations with at least three surveys were selected in this study to provide robust estimates of ground velocities. The observation time for each station exceeds 72 hr during each survey. All of the data were collected at similar time of year (around August) in order to decrease seasonal effects. A profile having a total of 27 GPS stations with dense near-field samples was constructed (Figure 1b).

Following the scheme presented by Gan et al. (2007), the GPS data were processed step by step as follows: (1) Using the GAMIT software, the raw GPS data were processed to obtain the loosely constrained daily coordinates and satellite orbits (Herring et al., 2010a). (2) These loosely constrained daily solutions were combined with the loosely constrained global solutions of 80 IGS tracking stations (released by Scripps Orbital and Position Analysis Center, http://sopac.ucsd.edu/) using the GLOBK software (Herring et al., 2010b), from which the solutions were fixed to the ITRF08 frame. (3) The station velocity and related uncertainty were solved through linear regression of the obtained GPS displacement time series. (4) The GPS velocities in ITRF08 were further translated to the fixed Eurasian frame based on the Euler parameters (Altamimi et al., 2012). (5) The horizontal velocities were projected onto the fault-parallel (N110°E) and the fault-perpendicular (N20°E) directions, respectively, in order to estimate the velocity gradient across the fault (Figure 1b and Table S1). Note that a few stations were affected by coseismic deformation of the 2001 Kunlun (Mw 7.8), 2008 Wenchuan (Mw 7.9), and 2010 Yushu (Mw 6.9) earthquakes. We calculated these effects using the published geodetic coseismic slip models (Lasserre et al., 2005; Z. Li, Elliott, et al., 2011; Wang et al., 2011) and removed them from the displacement time series. The final velocity profile shows

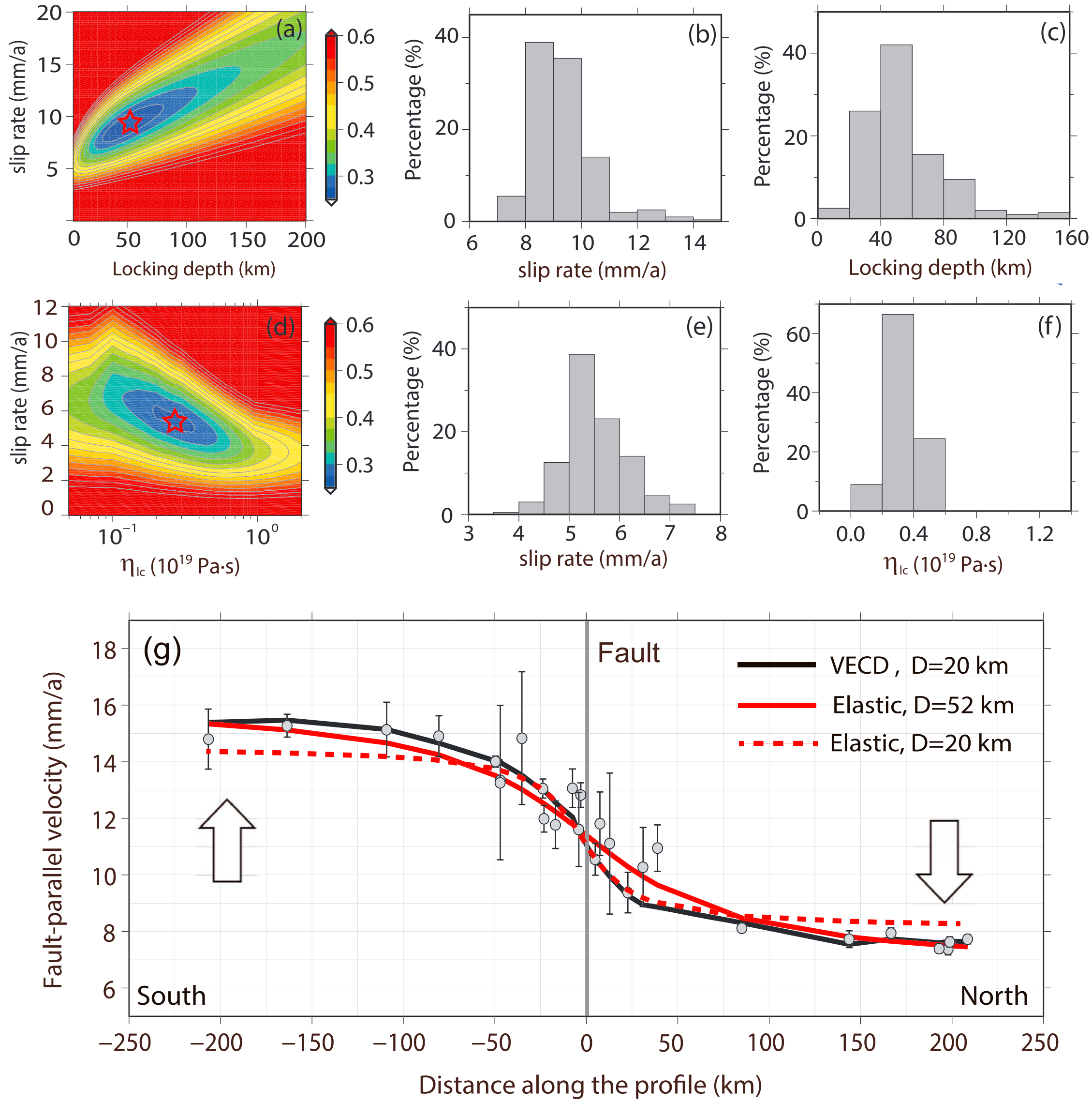

Figure 3. Inversion results based on the elastic and the viscoelastic models. (a) Misfit variance map (normalized by the data variance) of the elastic model (V_∞ vs. D). (b and c) The statistical distribution of the slip rate and locking depth inferred from 500 Monte Carlo simulations for the elastic model. (d) Misfit variance map of the viscoelastic earthquake-cycle deformation (VECD) model (V vs η_{lc}). (e and f) Similar to (b) and (c) but for the parameters of the VECD model. (g) Fault-parallel (N110°E) ground velocities with the gray dots showing the error bars (95% confidence interval). The solid black and red curves show the velocity profiles predicted from the optimal VECD model and elastic model, respectively. The dashed red curve is inferred from the best fit elastic model with a fixed locking depth of 20 km.

a clear velocity gradient in the fault-parallel direction (Figure 3g), suggesting significant strike-slip strain accumulation. In contrast, the identified fault-perpendicular velocity gradient is distributed in a broad region along the profile and no clear gradient is observed near the fault, revealing that the fault thrust-slip component on this segment might be negligible (Figure S1).

3. Elastic and Viscoelastic Models

3.1. Elastic Model

We first try to explain the observations using the simple elastic dislocation model proposed by Savage and Burford (1973). Based on this model, the fault-parallel velocity (V) is a function of distance perpendicular to the fault (x), interseismic locking depth (D), and long-term fault slip (V_∞),

$$V(x) = \frac{V_\infty}{\pi}\arctan\left(\frac{x}{D}\right). \tag{1}$$

The optimal values of V_∞ and D can be found through a grid search method. The uncertainty of the obtained (V_∞, D) is estimated statistically using the Monte Carlo method (Walters et al., 2011). For this purpose, we generate a set of Gaussian noise signals using the observation uncertainty as the standard deviation and add them to the data. For each of the disturbed data sets, we repeated the grid search process for the corresponding optimal V_∞ and D. These steps were run 500 times in order to estimate the uncertainty of the two parameters statistically.

3.2. VECD Model

Following the configuration used in previous studies (e.g., Dixon et al., 2003; Hilley et al., 2009; Meade & Hager, 2004; Savage & Prescott, 1978), our VECD model consists of the KLF embedded in an elastic upper crust overlying a lower crust and a half-space upper mantle, both of which are represented by linear Maxwell rheology (Figure 2). The model incorporates viscoelastic deformation driven by the periodic sudden slips (earthquake cycle) and continuous interseismic stress loading (constant back-slip rate) on each segment of the fault (Figure 2a). An earthquake represented by a sudden slip occurs at the beginning of a cycle, releasing the back-slip accumulated during the last cycle. After the sudden slip, the segment remains locked for the rest of the cycle. Both sudden slips and steady state back-slips cause stress variations in the viscoelastic lower crust and upper mantle, which are relaxed with time-dependent surface deformation in the postseismic and interseismic periods.

In the VECD model, the accumulated surface displacement field can be decomposed into three parts: (1) long-term plate motion, (2) coseismic and postseismic deformation induced by the periodic sudden slips, and (3) deformation due to the back-slip of faults, which are introduced to account for the effect of interseismic fault locking. Each fault segment is assumed to rupture periodically with its own recurrence interval. For simplicity, we only consider the past N earthquakes on each fault segment. Based on the assumptions, the accumulated surface displacement during the past N earthquake cycles can be expressed in the following form,

$$U(\boldsymbol{x}, t) = V(\boldsymbol{x})t + \sum_{i=1}^{L}\left[\sum_{n=0}^{N-1} V_i T_i G_i(\boldsymbol{x}, t-t_i + nT_i) - \int_0^t V_i G_i(\boldsymbol{x}, t-\tau)d\tau\right], \tag{2}$$

where $\boldsymbol{x}$ is the position of GPS stations, L is the total number of fault segments indexed with i, t is the time since the earliest event of the past N earthquake cycles indexed with n, t_i is the occurrence time of the latest earthquake ($n = 0$) on the ith fault segment, V is the long-term velocity of plate motion, V_i is the long-term slip rate given by the relative plate motion along the fault, T_i is the earthquake recurrence interval, and G_i is Green's function representing the elastic and viscoelastic displacement caused by a unit slip on the ith fault segment.

The long-term plate motion is estimated following a strategy similar to that used in the 1-D elastic earthquake cycle model but considering the variable slip rates along the fault. For this purpose, we include deep slip below the seismogenic zone (0–20 km) to a large enough depth (here 5,000 km). To decrease the lateral boundary effect, we additionally extend the length of both eastern and western edge segments by 1,000 km, respectively. As shown by Klein et al. (2017), the plate motion predicted by this strategy is more realistic than that predicted by the 1-D model with a uniform slip rate and an infinite fault length.

In contrast to the steady state plate motion, the viscoelastic effect should be considered when calculating Green's function for surface displacement caused by fault slips. In general, Green's function can be separated into the elastic part and the viscoelastic part

$$G(\boldsymbol{x}, t) = [C(\mathbf{x}) + P(\boldsymbol{x}, t)]H(t), \tag{3}$$

where $H(t)$ is the Heaviside function, $C(\boldsymbol{x})$ is the elastic displacement, and $P(\boldsymbol{x}, t)$ is the time-dependent displacement induced by viscoelastic relaxation in the lower crust and upper mantle. Note that not only the sudden slip but also the continuous slip accumulation (*back-slip*) can cause stress change and result in viscoelastic relaxation.

Using equation (3), the back-slip term in equation (2) can be reformulated to

$$-\int_0^t V_i G_i(\boldsymbol{x}, t-\tau)d\tau = -V_i\left[C_i(\boldsymbol{x})t + \int_0^t P_i(\boldsymbol{x}, \tau)d\tau\right], \tag{4}$$

and after a large enough number of cycles ($N \rightarrow \infty$), the ground velocity is calculated by

$$\frac{\partial}{\partial t}U(\boldsymbol{x}, t) = \left[V(\boldsymbol{x}) - \sum_{i=1}^{L} V_i C_i(\boldsymbol{x})\right] + \sum_{i=1}^{L} V_i\left[T_i \sum_{n=0}^{\infty} \frac{\partial}{\partial t} P_i(\boldsymbol{x}, t-t_i + nT_i) - P_i(\boldsymbol{x}, \infty)\right], \tag{5}$$

The two terms in the first brackets on the right-hand side of equation (5) are the plate motion and the elastic part of interseismic deformation, respectively. The other terms represent the viscoelastic part of sudden slips and continuous back-slips. At distances far enough away from the fault, both elastic and viscoelastic deformation parts become negligible and the ground velocity converges to that of the long-term plate motion. Furthermore, it can be easily shown that the viscoelastic part makes no net contribution to the accumulative displacement during a complete earthquake cycle because for each fault segment it is valid that

$$\begin{aligned}
&\int_{t_i}^{t_i+T_i}\left\{T_i \sum_{n=0}^{\infty} \frac{\partial}{\partial t} P_i(\boldsymbol{x}, t-t_i + nT_i) - P_i(\boldsymbol{x}, \infty)\right\}dt \\
&= T_i\left\{\sum_{n=0}^{\infty}\{P_i[\boldsymbol{x}, (n+1)T_i] - P_i(\boldsymbol{x}, nT_i)\} - P_i(\boldsymbol{x}, \infty)\right\} \\
&= T_i[P_i(\boldsymbol{x}, \infty) - P_i(\boldsymbol{x}, \infty)] \\
&= 0.
\end{aligned} \tag{6}$$

Note that here we have used $P_i(\boldsymbol{x}, 0) = 0$. Generally, the viscoelastic effect speeds up the interseismic ground velocity in the early stage of the cycle and slows down it in the late stage of the cycle, independently of the viscoelastic structure and the fault configuration as well as the slip distribution on it.

Based on the theory derived above, we use the PSGRN/PSCMP code (Wang et al., 2006) to calculate the ground velocity for a layered viscoelastic model. Forward simulation tests reveal that the surface velocity throughout an earthquake cycle converges when N is larger than 10 for the present case. To identify the reliability of the simulation, we compare the results with those inferred from Savage and Prescott (1978) based on a simple two-layer Nur-Mavko model with a single fault segment of infinite length. As shown in Figure S2, our numerical results show an excellent agreement with the analytical solution obtained by Savage and Prescott (1978).

In our VECD model, the crustal velocity depends on parameters (V, T) of each fault segment and viscosities of the lower crust (η_{lc}) and upper mantle (η_{um}). The parameter setting of each fault segment is shown in Table S2 as inferred from previous studies (Guo et al., 2006; Li et al., 2005; C. Li, Xu, et al., 2011; Lin et al., 2002; Van der Woerd et al., 1998, 2000, 2002). The occurrence interval of the TL segment (T_{TL}) is set to 630 years based on the geological investigation (C. Li, Xu, et al., 2011), whereas the slip rate of the Tuosuo segment (V_{TL}) remains to be solved. We set the thickness of the elastic layer (D) to 20 km based on the 95% of focal depths of seismicity in this area (Figure S3) and the estimate of coseismic rupture depth (Lasserre et al., 2005). The viscosity η_{um} is fixed to 1.0×10^{20} Pas based on the previous studies on postseismic deformation in this region (Ryder et al., 2011; Wen et al., 2012). The effects induced by the uncertainties of T_{TL}, η_{um}, and D are further tested and discussed in the next section. After fixing most of the parameters of the model, we adjust η_{lc} and V_{TL} and find the optimal values by minimizing the misfit between the observed velocity (V_{obs}) and the model prediction (V_{model}) again by the grid search method as used for the elastic model,

$$F(\eta_{\mathrm{lc}}, V_{\mathrm{TL}}) = \sum_{j=1}^{J} \sigma_j^{-2}\left[V_{\mathrm{obs},j} - V_{\mathrm{model},j}(\eta_{\mathrm{lc}}, V_{\mathrm{TL}})\right]^2 \tag{7}$$

where j is the index of the GPS station and σ is the measurement error of observed velocities. Note that the large-scale crustal shorting in the fault-perpendicular direction of the study area is subjected to large-scale tectonic deformation (Zhang et al., 2004). Therefore, only the fault-parallel components of GPS velocities are employed to constrain the model parameters. The same approach as described in section 3.1 is used to estimate the uncertainties of the parameters.

4. Results and Discussion

4.1. Results and Robustness

Based on the simplified 1-D elastic model, the V_{TL} is estimated to be 9.2 ± 1.1 mm/a (Figures 3a–3c), which is close to the geological slip rate (11.5 ± 2.0 mm/a) obtained by Van der Woerd et al., 2000, 2002), but higher than that (6.5 ± 1.1 mm/a) obtained by Guo et al. (2007). Moreover, the inferred corresponding fault locking depth of 52.0 ± 24.7 km is well beyond the seismogenic thickness of this region (~20 km). In comparison, the optimal VECD model yields a fault slip rate of 5.5 ± 0.7 mm/a (Figures 3d–3f), which is significantly lower than the geological estimate of Van der Woerd et al. (2000, 2002) but is consistent with the estimate of Guo et al. (2007). The corresponding η_{lc} is estimated to be ~ 3.0×10^{18} Pa · s, which agrees well with the values derived from postseismic observations in this region (e.g., Ryder et al., 2011; Wen et al., 2012). The variance reduction of the optimal elastic and viscoelastic models is close to 95%, resulting in a root-mean-square misfit of less than 1 mm/a, which locates within the uncertainty of the observations. Besides, we also tried fixing the locking depth at 20 km for the elastic model; however, it yields a slip rate of 7.0 mm/a that significantly underestimates the far-field velocities (Figure 3g). Therefore, the results inferred from the VECD model should be more reasonable in terms of the more realistic model configuration, that is, incorporation of viscoelastic effect and variable slip rate along the fault.

For a robust estimation of V_{TL} and η_{lc} in the VECD model, the fixed parameters (η_{um}, T_{TL}, and D) are tested to identify their effects, separately. No significant variations are observed in the inferred V_{TL} and η_{lc} by changing η_{um} (Figure S4), suggesting that the VECD model is not sensitive to η_{um}. However, the V_{TL} decreases from 6.2 ± 0.9 mm/a to 4.3 ± 0.6 mm/a by increasing T_{TL} from 500 to 760 years (Figure S5), implying a moderate trade-off between the parameters T_{TL} and V_{TL}. Moreover, the estimated V_{TL} are 5.1 ± 0.6 mm/a, 5.5 ± 0.7 mm/a, and 7.5 ± 0.8 mm/a when fixing D to 15, 20, and 30 km (Figure S6), indicating that an increased D will decrease the viscoelastic effects and make the solution close to that of the elastic models (Savage & Prescott, 1978). Besides, the model with $D = 20$ km can explain the data better (with small misfit) than that with $D = 15$ km or $D = 30$ km, suggesting that the parameter inferred from a prior information is reasonable.

Note that we fix T, D, and V (adjacent segments) based on a priori information and neglect the lateral variation of viscosity structure to make a first-order approximation. As shown by the sensitivity tests and previous studies (e.g., Hetland & Hager, 2006; Ryder et al., 2011), these simplifications may potentially affect the parameter estimation and lead to underestimated uncertainties of the inferred V_{TL}. Further investigations with better spatial and temporal data coverage may allow more detailed analysis of these parameters.

4.2. Cross-Fault Deformation throughout the Earthquake Cycle

The V_{TL} inferred from the elastic model is clearly larger than that deduced from the VECD model. The difference highlights the overlapping viscoelastic effects on geodetic fault slip rate estimate during the earthquake cycle. To show the time-dependent velocities across the fault, we simulate a complete earthquake cycle using the obtained VECD model. Immediately after an event the inferred cross-fault velocity is clearly faster than the reference steady state velocity inferred from a corresponding elastic model (Figure S7). At $t \geq 0.3T$, the VECD velocity is slightly smaller and has a lower gradient than that given by the elastic reference. These results suggest that overestimation and underestimation of the fault slip rate would be inevitable in the early and late stages of an earthquake cycle if the viscoelastic effects were ignored. For the present case of the TL segment, the occurrence of the 1937 Huashixia earthquake yields $t/T \approx 0.1$ at the observation time. Such a scenario leads to a highly overestimated slip rate by neglecting the viscoelastic effect (i.e., overestimation at the early stage of a cycle). Furthermore, we show the contributions of different deformation components (see equation (5)) in Figure S8.

4.3. Tectonic Implications of the Slip Rate Variation along the Kunlun Fault

The mechanism of the slip rate variation along the KLF remains controversial. Kirby et al. (2007) suggest that the rapidly decreasing fault slip is mainly absorbed by internal deformation and thickening of the

10.1029/2019GL081940

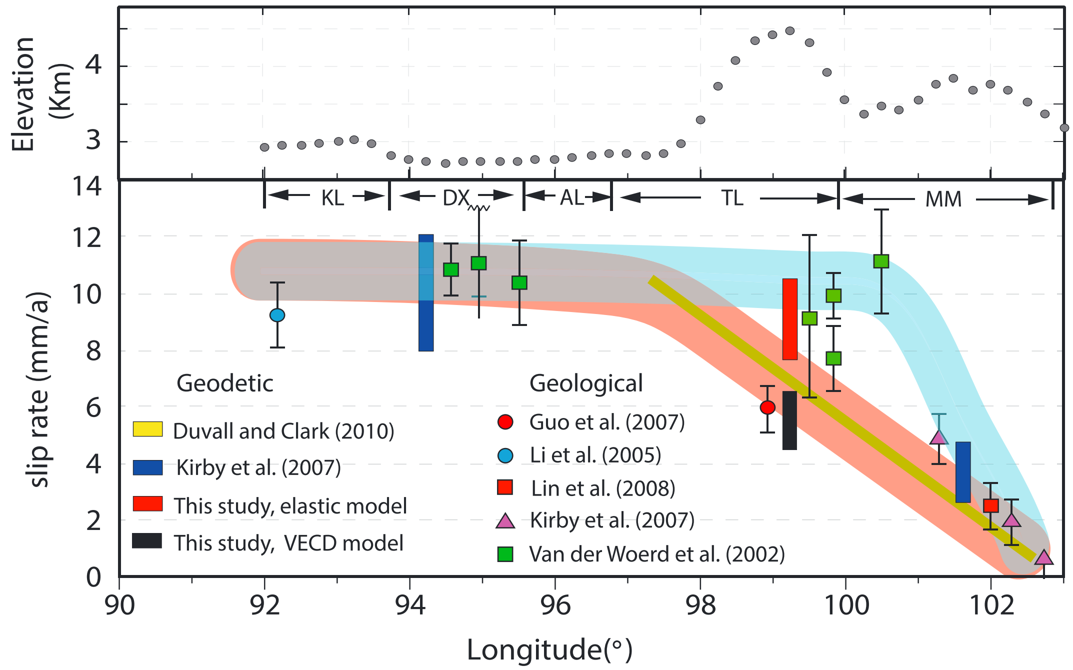

Figure 4. Slip rate variations along the Kunlun fault inferred from geological and geodetic investigations (lower panel). The shaded red belt shows the slip rate variations along the Kunlun fault based on the results of previous studies and this study. The shaded blue belt shows the slip rate variation model proposed by Kirby et al. (2007). The upper panel shows the elevation along a 100-km-wide zone north of the fault.

plateau surrounding the fault tip. Duvall and Clark (2010) consider that the systematically decreasing slip along the KLF is transformed to the slip of the northern Haiyuan fault and distributed deformation in the step-over region between them, rather than transformed to the east margin of the Tibetan Plateau. C. Li, Xu, et al. (2011) infer that the slip rate decrease is mainly transformed to transverse secondary faults and crust deformation near fault bends. The slip rate inferred from the VECD model in this study supports the view of systematic slip rate decrease along the KLF (Duvall & Clark, 2010). Moreover, the relief variations at the north side along the fault show spatial agreement with systematic slip rate decrease (Figure 4, upper panel), suggesting that the crustal thickening and internal deformation around the eastern fault segment may absorb part of the decreased fault slip. However, the hypotheses mentioned above are not mutually exclusive, and it is possible that each mechanism is acting (Kirby et al., 2007). Further investigations, such as more geodetic observations surrounding the fault and numerical simulations of fault interactions, are required to test these hypotheses.

Similar slip rate gradient has been observed on the northern Altyn Tagh fault and Haiyuan fault, of which the slip rates decrease gradually toward the eastern tip (Zhang et al., 2007; Zheng et al., 2013). Such slip rate variations of large strike-slip faults may obey a scaling relationship between fault displacement and length, which suggests that the slip rate decrease can generally be observed from the central segment toward the fault tip as inferred from investigations of several faults worldwide (Cowie & Scholz, 1992; Stirling et al., 1996).

5. Conclusions

Constrained by a dense GPS velocity profile, the V_{TL} of the KLF was investigated with a VECD model. The inferred V_{TL} of 5.5 ± 0.7 mm/a is consistent with the previous first-order geodetic results (Duvall & Clark, 2010) and the geological estimate (Guo et al., 2007). An overestimated V_{TL} of 9.2 ± 1.1 mm/a is predicted using an elastic model, indicating that viscoelastic effects should be considered for analyzing the geodetic observations at the interseismic stage of an earthquake cycle. Combining previous results with those from this study, we infer that the slip rate of the KLF may decrease gradually from the TL segment toward the eastern tip, which contradicts previous views that suggest a uniform slip rate along the fault or a rapidly decreasing slip rate within the easternmost 150 km of the fault. The obtained η_{lc} agrees with values inferred from postseismic studies in this region; both are on the order of 10^{18} Pa · s, suggesting a weak ductile lower crust beneath the elastic seismogenic layer.

Acknowledgments
All data supporting the conclusion of this paper are available in Table S1. This work was supported by the National Key R & D Program of China (grants 2017YFC1500501 and 2017YFC1500305) funded by the Ministry of Science and Technology of the People's Republic of China (MOST) and the National Natural Science Foundation of China (grants 41674023, 41304017, and 41731072). Some of the data used were obtained from the Crustal Movement Observation Network of China (CMONOC). We thank Thorne Lay for carefully polishing the paper and XingXing Li and Kejie Chen for help in GPS data processing. We thank Shaoyang Li and one anonymous reviewer for valuable comments. The figures were drawn using the Generic Mapping Tools (GMT) software (Wessel & Smith, 1998).

References

Altamimi, Z., Métivier, L., & Collilieux, X. (2012). ITRF2008 plate motion model. *Journal of Geophysical Research*, *117*, B07402. https://doi.org/10.1029/2011JB008930

Cowie, P. A., & Scholz, C. H. (1992). Displacement length scaling relationship for faults: Data synthesis and discussion. *Journal of Structural Geology*, *14*(10), 1149–1156. https://doi.org/10.1016/0191-8141(92)90066-6

Diao, F., Walter, T. R., Solaro, G., Wang, R., Bonano, M., Manzo, M., et al. (2016). Fault locking near Istanbul: Indication of earthquake potential from InSAR and GPS observations. *Geophysical Journal International*, *205*(1), 490–498. https://doi.org/10.1093/gji/ggw048

Dixon, T. H., Norabuena, E., & Hotaling, L. (2003). Paleoseismology and Global Positioning System: Earthquake-cycle effects and geodetic versus geologic fault slip rates in the Eastern California shear zone. *Geology*, *31*(1), 55–58. https://doi.org/10.1130/0091-7613

Duvall, A. R., & Clark, M. K. (2010). Dissipation of fast strike-slip faulting within and beyond northeastern Tibet. *Geology*, *38*(3), 223–226. https://doi.org/10.1130/G30711.1

Gan, W., Zhang, P., Shen, Z. K., Niu, Z., Wang, M., Wan, Y., et al. (2007). Present-day crustal motion within the Tibetan Plateau inferred from GPS measurements. *Journal of Geophysical Research*, *112*, B08416. https://doi.org/10.1029/2005JB004120

Guo, J., Lin, A., Maruyama, T., Zheng, J., & Sun, G. (2006). New constraints on recent large earthquakes along the Xidatan-Dongdatan segment of the Kunlun fault, western China. *Bulletin of the Seismological Society of America*, *96*(1), 48–58. https://doi.org/10.1785/0120040176

Guo, J., Lin, A., Sun, G., & Zheng, J. (2007). Surface ruptures associated with the 1937 M 7.5 Tuosuo Lake earthquake and the 1963 M7.0 Alake Lake earthquake and the paleoseismicity along the Tuosuo Lake segment of the Kunlun fault, northern Tibet. *Bulletin of the Seismological Society of America*, *97*(2), 474–496. https://doi.org/10.1785/0120050103

Herring, T. A., King, R.W., & McClusky, S. C. (2010a). GAMIT reference manual. GPS Analysis at MIT. Release 10.4. Massachussetts Institute Technology. Retrieved from http://www-gpsg.mit.edu/~simon/gtgk/index.htm

Herring, T. A., King, R.W., & McClusky, S. C. (2010b). GLOBK reference manual: Global Kalman filter VLBI and GPS analysis program. Release 10.4. Massachusetts Institute of Technology. Retrieved from http://www-gpsg.mit.edu/~simon/gtgk/index.htm

Hetland, E., & Hager, B. (2006). Interseismic strain accumulation: Spin-up, cycle invariance, and irregular rupture sequences. *Geochemistry, Geophysics, Geosystems*, *7*, Q05004. https://doi.org/10.1029/2005GC001087

Hilley, G. E., Johnson, K. M., Wang, M., Shen, Z. K., & Bürgmann, R. (2009). Earthquake cycle deformation and fault slip rates in northern Tibet. *Geology*, *37*(1), 31–34. https://doi.org/10.1130/G25157A.1

Hubbard, J., Almeida, R., Foster, A., Sapkota, S. N., Bürgi, P., & Tapponnier, P. (2016). Structural segmentation controlled the 2015 Mw 7.8 Gorkha earthquake rupture in Nepal. *Geology*, *44*(8), 639–642. https://doi.org/10.1130/G38077.1

Johnson, K. M., Hilley, G. E., & Bürgmann, R. (2007). Influence of lithosphere viscosity structure on estimates of fault slip rate in the Mojave region of the San Andreas fault system. *Journal of Geophysical Research*, *112*, B07408. https://doi.org/10.1029/2006JB004842

Kirby, E., Harkins, N., Wang, E., Shi, X., Fan, C., & Burbank, D. (2007). Slip rate gradients along the eastern Kunlun fault. *Tectonics*, *26*, TC2010. https://doi.org/10.1029/2006TC002033

Klein, E., Duputel, Z., Masson, F., Yavasoglu, H., & Agram, P. (2017). Aseismic slip and seismogenic coupling in the Marmara Sea: What can we learn from onland Geodesy? *Geophysical Research Letters*, *44*, 3100–3108. https://doi.org/10.1002/2017GL072777

Lasserre, C., Peltzer, G., Crampé, F., Klinger, Y., Van der Woerd, J., & Tapponnier, P. (2005). Coseismic deformation of the 2001 Mw = 7.8 Kokoxili earthquake in Tibet, measured by synthetic aperture radar interferometry. *Journal of Geophysical Research*, *110*, B12408. https://doi.org/10.1029/2004JB003500

Li, C. X., Xu, X., Wen, X., Zheng, R., Chen, G., Yang, H., et al. (2011). Rupture segmentation and slip partitioning of the mid-eastern part of the Kunlun fault, north Tibetan Plateau. *Science China Earth Sciences*, *54*(11), 1730–1745. https://doi.org/10.1007/s11430-011-4239-5

Li, H., Van der Woerd, J., Tapponnier, P., Klinger, Y., Qi, X., Yang, J., & Zhu, Y. (2005). Slip rate on the Kunlun fault at Hongshui Gou, and recurrence time of great events comparable to the 14/11/2001, Mw = 7.9 Kokoxili earthquake. *Earth and Planetary Science Letters*, *237*(1-2), 285–299. https://doi.org/10.1016/j.epsl.2005.05.041

Li, Z., Elliott, J. R., Feng, W., Jackson, J. A., Parsons, B. E., & Walters, R. J. (2011). The 2010 MW 6.8 Yushu (Qinghai, China) earthquake: Constraints provided by InSAR and body wave seismology. *Journal of Geophysical Research*, *116*, B10302. https://doi.org/10.1029/2011JB008358

Lin, A., Fu, B., Guo, J., Zeng, Q., Dang, G., He, W., & Zhao, Y. (2002). Co-seismic strike-slip and rupture length produced by the 2001 Ms 8.1 central Kunlun earthquake. *Science*, *296*(5575), 2015–2017. https://doi.org/10.1126/science.1070879

Lin, A., & Guo, J. (2008). Nonuniform slip rate and millennial recurrence interval of large earthquakes along the eastern segment of the Kunlun fault, northern Tibet. *Bulletin of the Seismological Society of America*, *98*(6), 2866–2878. https://doi.org/10.1785/0120070193

Manighetti, I., Campillo, M., Bouley, S., & Cotton, F. (2007). Earthquake scaling, fault seg-mentation, and structural maturity. *Earth and Planetary Science Letters*, *253*(3–4), 429–438. https://doi.org/10.1016/j.epsl.2006.11.004

Meade, B. J., & Hager, B. H. (2004). Viscoelastic deformation for a clustered earthquake cycle. *Geophysical Research Letters*, *31*, L10610. https://doi.org/10.1029/2004GL019643

Pollitz, F. F. (2001). Viscoelastic shear zone model of a strike-slip earthquake cycle. *Journal of Geophysical Research*, *106*(B11), 26,541–26,560. https://doi.org/10.1029/2001JB000342

Ryder, I., Bürgmann, R., & Pollitz, F. (2011). Lower crustal relaxation beneath the Tibetan Plateau and Qaidam Basin following the 2001 Kokoxili earthquake. *Geophysical Journal International*, *187*(2), 613–630. https://doi.org/10.1111/j.1365-246X.2011.05179.x

Savage, J. C. (2000). Viscoelastic-coupling model for the earthquake cycle driven from below. *Journal of Geophysical Research*, *105*(B11), 25,525–25,532. https://doi.org/10.1029/2000JB900276

Savage, J. C., & Burford, R. O. (1973). Geodetic determination of the relative plate motion in central California. *Journal of Geophysical Research*, *78*(5), 832–845. https://doi.org/10.1029/JB078i005p00832

Savage, J. C., & Prescott, W. (1978). Asthenosphere readjustment and the earthquake cycle. *Journal of Geophysical Research*, *83*(B7), 3369–3376. https://doi.org/10.1029/JB083iB07p03369

Segall, P., & Pollard, D. D. (1980). Mechanics of discontinuous faults. *Journal of Geophysical Research*, *85*(B8), 4337–4350. https://doi.org/10.1029/JB085iB08p04337

Stirling, M. K., Wesnousky, S. G., & Shimzaki, K. (1996). Fault trace complexity, cumulative slip, and the shape of the magnitude-frequency distribution for strike-slip faults: A global survey. *Geophysical Journal International*, *124*(3), 833–868. https://doi.org/10.1111/j.1365-246X.1996.tb05641.x

Van der Woerd, J., Ryerson, F. J., Tapponnier, P., Gaudemer, Y., Finkel, R. C., Meriaux, A.-S., et al. (1998). Holocene left slip-rate determined by cosmogenic surface dating on the Xidatan segment of the Kunlun fault (Qinghai, China). *Geology*, *26*(8), 695–698. https://doi.org/10.1130/0091-7613(1998)026<0695:HLSRDB>2.3.CO;2

Van der Woerd, J., Ryerson, F. J., Tapponnier, P., Meriaux, A. S., Gaudemer, Y., Meyer, B., et al. (2000). Uniform slip-rate along the Kunlun fault: Implications for seismic behavior and large-scale tectonics. *Geophysical Research Letter*, *27*(16), 2353–2356. https://doi.org/10.1029/1999GL011292

Van der Woerd, J., Tapponnier, P., Ryerson, F. J., Meriaux, A. S., Meyer, B., Gaudemer, Y., et al. (2002). Uniform postglacial slip-rate along the central 600 km of the Kunlun fault (Tibet), from ^{26}Al, ^{10}Be, and ^{14}C dating of riser offsets, and climatic origin of the regional morphology. *Geophysical Journal International*, *148*(3), 356–388. https://doi.org/10.1046/j.1365-246x.2002.01556.x

Walters, R. J., Holley, R. J., Parsons, B., & Wright, T. J. (2011). Interseismic strain accumulation across the North Anatolian Fault from Envisat InSAR measurements. *Geophysical Research Letters*, *38*, L05303. https://doi.org/10.1029/2010GL046443

Wang, K., Hu, Y., & He, J. (2012). Deformation cycles of subduction earthquakes in a viscoelastic Earth. *Nature*, *484*(7394), 327–332. https://doi.org/10.1038/nature11032

Wang, Q., Qiao, X., Lan, Q., Jeffrey, F., Yang, S., Xu, C., et al. (2011). Rupture of deep faults in the 2008 Wenchuan earthquake and uplift of the 604 Longmen Shan. *Nature Geoscience*, *4*(9), 634–640. https://doi.org/10.1038/NGEO1210

Wang, R., Lorenzo-Martin, F., & Roth, F. (2006). PSGRN/PSCMP—A new code for calculating co- and post-seismic deformation, geoid and gravity changes based on the viscoelastic-gravitational dislocation theory. *Computer and Geoscience*, *32*(4), 527–541. https://doi.org/10.1016/j.cageo.2005.08.006

Wen, Y., Li, Z., Xu, C., Ryder, I., & Bürgmann, R. (2012). Postseismic motion after the 2001 MW 7.8 Kokoxili earthquake in Tibet observed by InSAR time series. *Journal of Geophysical Research*, *117*, B08405. https://doi.org/10.1029/2011JB009043

Wessel, P., & Smith, W. H. F. (1998). New improved version of Generic Mapping Tools released. *Eos, Transactions American Geophysical Union*, *79*(47), 579. https://doi.org/10.1029/98EO00426

Xiong, X., Shan, B., Zheng, Y., & Wang, R. (2010). Stress transfer and its implication for earthquake hazard on the Kunlun fault, Tibet. *Tectonophysics*, *482*(1-4), 216–225. https://doi.org/10.1016/j.tecto.2009.07.020

Zhang, P., Shen, Z., Wang, M., Gan, W., Bürgmann, R., Molnar, P., et al. (2004). Continuous deformation of the Tibetan Plateau from Global Positioning System data. *Geology*, *32*(9), 809–812. https://doi.org/10.1130/G20554.1

Zhang, P. Z., Molnar, P., & Xu, X. (2007). Late Quaternary and present-day rates of slip along the Altyn Tagh fault, northern margin of the Tibetan Plateau. *Tectonics*, *26*, TC5010. https://doi.org/10.1029/2006TC002014

Zheng, W., Zhang, P., He, W., Yuan, D., Shao, Y., Zheng, D., et al. (2013). Transformation of displacement between strike-slip and crustal shortening in the northern margin of the Tibetan Plateau: Evidence from decadal GPS measurements and late Quaternary slip rates on faults. *Tectonophysics*, *584*, 267–280. https://doi.org/10.1016/j.tecto.2012.01.006